

Enhanced linear and nonlinear optical phase response of AlGaAs microring resonators

John E. Heebner,* Nick N. Lepeshkin, Aaron Schweinsberg, G. W. Wicks, and Robert W. Boyd

The Institute of Optics, University of Rochester, Rochester, New York 14627

Rohit Grover[†] and P.-T. Ho

The Laboratory for Physical Sciences, 8050 Greenmead Drive, College Park, Maryland 20740

Received October 29, 2003

We have constructed and characterized several optical microring resonators with scale sizes of the order of 10 μm . These devices are intended to serve as building blocks for engineerable linear and nonlinear photonic media. Light is guided vertically by an epitaxially grown structure and transversely by deeply etched air-clad sidewalls. We report on the spectral phase transfer characteristics of such resonators. We also report the observation of a π -rad Kerr nonlinear phase shift accumulated in a single compact ring resonator evidenced by all-optical switching between output ports of a resonator-enhanced Mach-Zehnder interferometer. © 2004 Optical Society of America

OCIS codes: 190.4390, 190.4360, 130.3120, 130.3750, 190.3270, 130.5990.

In recent years optical microring resonators have become an intense area of active research. Much of this activity centers on a potential for highly compact add-drop filter networks,^{1,2} dispersion compensators,³ delay lines,⁴ and sensors.^{5,6} Microring resonators can also serve as key elements in the realization of engineerable photonic media. A sequence of resonators coupled to an optical waveguide can be viewed as an optical transmission line with highly controllable dispersive and nonlinear properties similar to those of photonic crystals. In previous articles^{7,8} many applications of these artificial channels were proposed ranging from soliton propagation on a chip to miniaturized all-optical switches, delay lines, and pulse compressors. Most of these applications require nonlinear phase shifts near π rad to become practical, and such was the goal of this experimental work.

Recently, all-optical switching in a single GaAs-guiding microresonator was observed for the first time.⁹ In this work we chose to construct ring resonators in AlGaAs and probe them at a photon energy ($hc/\lambda = 0.8$ eV) below the half-gap ($E_g/2 = 0.97$ eV) of the material. Our motivation for this choice was to maximize the ultrafast bound (Kerr) nonlinearities resulting from virtual transitions while minimizing the two-photon contribution to carrier generation.¹⁰ Although this effect is a relatively weak nonlinearity requiring higher circulating intensities than in the previous work, the deposition of heat resulting from two-photon absorption can be substantially minimized. In addition, the lower limit of response time is dictated by the cavity lifetime only and not the carrier recombination lifetime.

Ring resonators are ideal candidates for the miniaturization of photonic devices because they have the ability to recycle light through feedback and thus demand less physical path length to exhibit certain linear optical effects. The coherent buildup of inten-

sity circulating within the resonator further reduces the required path length (or intensity) for accessing traditionally weak nonlinear optical effects. Applied to the case of Kerr nonlinear phase accumulation, which scales with the product of length and intensity, it has been shown that nonlinear phase shifts are enhanced in proportion to the square of the resonator finesse.¹¹

The transmission of a microring-based add-drop resonator can be modeled according to

$$\mathcal{T} = \frac{r_2^2 - 2r_1r_2 \cos \phi + r_1^2}{1 - 2r_1r_2 \cos \phi + r_1^2r_2^2}, \quad (1)$$

where $\phi = T_R \Delta\omega$ is the detuning $\Delta\omega$ from resonance normalized by the ring transit time T_R , and r_1 and r_2 are the self-coupling coefficients. The resonator finesse is given by $\mathcal{F} \approx \pi/(1 - r_1r_2)$. Setting $r_2 = 1$ is equivalent to removing one of the coupled waveguides and results in the classic all-pass, phase-only resonator. While maintaining a unit-amplitude transmission spectrum, the transmitted phase of this device varies as

$$\Phi = \pi + \phi + 2 \arctan\left(\frac{r \sin \phi}{1 - r \cos \phi}\right). \quad (2)$$

Because of an increased phase sensitivity (or increased effective path length) near resonance, the resonator need only be detuned by $2\pi/\mathcal{F}$ rad to achieve a net transmitted phase shift of π . Furthermore, the power threshold requirement to achieve this detuning by means of an intensity-dependent refractive-index change is reduced by a circulating intensity buildup of $B = 2\mathcal{F}/\pi$ so that

$$P_{\text{threshold}} \approx \frac{\pi \lambda A_{\text{eff}}}{2n_2 L \mathcal{F}^2}, \quad (3)$$

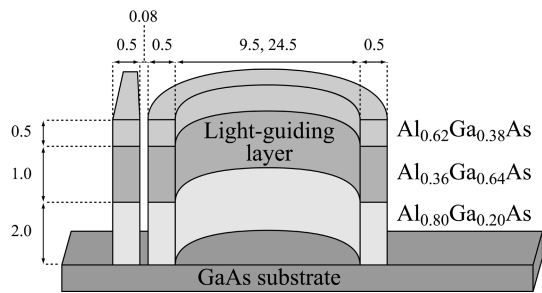


Fig. 1. Design of the resonator structures investigated in this work. The vertical structure is formed by molecular-beam epitaxy, and the horizontal structure by nanolithography. All dimensions are in micrometers.

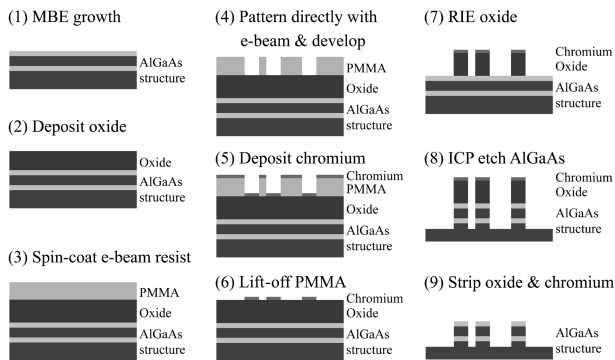


Fig. 2. Procedure used to fabricate the microresonators. MBE, molecular-beam epitaxy; RIE, reactive-ion etch; e-beam, electron-beam.

where A_{eff} is the effective mode area and L is the circumference. For a typical AlGaAs channel waveguide with a nonlinear coefficient of $n_2 = 10^{-17} \text{ m}^2/\text{W}$, an effective mode area of $0.5 \mu\text{m}^2$, a ring diameter of $10 \mu\text{m}$, and a finesse of 10, the threshold peak power is approximately 40 W at $1.55 \mu\text{m}$. Note that in comparison with standard single-mode silica fiber with a threshold power-length product of 500 Wm , this situation corresponds to $1200 \text{ W}\mu\text{m}$. This reduction of an order of magnitude of nearly 6 is attributed to a stronger nonlinear coefficient, a tighter mode area, and resonant enhancement.

We next describe the procedure used to fabricate the resonators. First, a vertically layered structure supporting guided waves was grown by means of molecular-beam epitaxy on a GaAs substrate. The arrangement of the layers and their composition are shown in Fig. 1. The lateral patterning procedure (see Fig. 2) is adapted from Ref. 12, which begins with the use of electron-beam lithography (Leica VB6) to define guiding regions in a poly(methyl methacrylate) (PMMA) resist and ends with a highly anisotropic inductively coupled plasma (ICP) etch into the AlGaAs. An intermediate oxide-chromium mask was used because the resist itself was not sufficiently robust to serve as a high-quality mask for deep anisotropic etching. Lift-off of the bilayer PMMA resist yielded a 40-nm chromium mask for reactive-ion etching of the underlying 800-nm oxide layer. Finally, the chlorine-based ICP etch transferred the pattern directly into the AlGaAs with highly vertical sidewalls.

Figure 3 displays scanning electron microscopy images of two of the fabricated devices. The narrow gap region was extended along the propagation direction by $4 \mu\text{m}$ into a racetrack geometry to increase the guide-to-ring coupling. Devices with varying gap width were fabricated and the best were selected during characterization.

To deliver light to the microresonator-based devices, the bus waveguides were tapered out to cleaved sample edges for a total sample length of 1 mm. Light was end-fire coupled into the tapered waveguides and collected at the other end with $40\times$ microscope objectives. A polarization controller was used to select TM excitation (field perpendicular to the plane of the ring). Spectral characterization of the microresonators was performed with a tunable diode laser near $1.55 \mu\text{m}$.

Figure 4 displays the spectral transmission data for the through port of the add-drop resonator in Fig. 3(a). Here, a racetrack resonator of $12.5\text{-}\mu\text{m}$ radius with extended straight segments coupled to two waveguides on either side has a measured bandwidth of 110 GHz, a free spectral range of 1.1 THz, and a finesse of approximately 10 ($Q = 1760$). Scattering-limited losses resulting from sidewall roughness are estimated at 10% per round trip.

Figure 5 displays the spectral transmission data for an output port of a nearly balanced Mach-Zehnder interferometer containing an all-pass resonator in one arm, as shown in Fig. 3(b). In this configuration the overcoupled phase response of the $5\text{-}\mu\text{m}$ radius racetrack resonator could be inferred from the amplitude response of the composite resonator-enhanced Mach-Zehnder (REMZ) interferometer. A

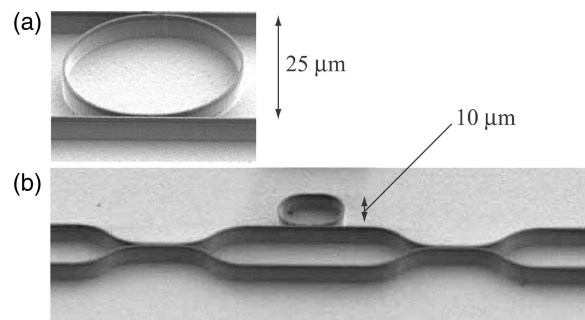


Fig. 3. Scanning electron microscopy images of (a) an add-drop ring resonator and (b) an all-pass ring resonator coupled to one arm of a Mach-Zehnder interferometer.

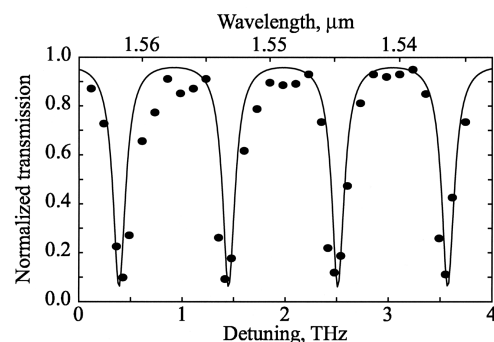


Fig. 4. Measured transmission spectrum of the microresonator shown in Fig. 3(a) with a theoretical fit.

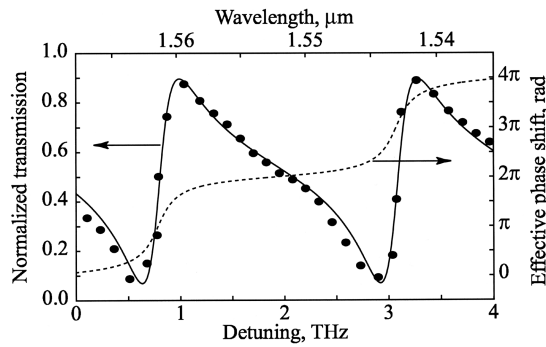


Fig. 5. Measured transmission spectrum (left axis) of the device shown in Fig. 3(b) with a theoretical fit. The resonator-induced phase shift as inferred from the interferogram is also shown in the plot (right axis).

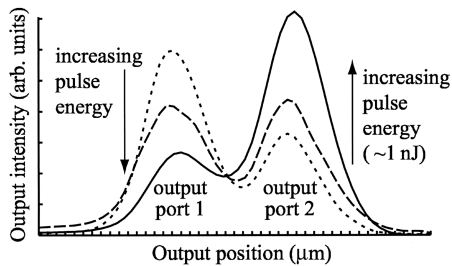


Fig. 6. Demonstration of all-optical switching between ports of a Mach-Zehnder interferometer resulting from the accumulation of a π -rad phase shift in a ring resonator [device shown in Fig. 3(b)].

measured bandwidth of 240 GHz and a free spectral range of 2.3 THz results in a finesse of approximately 10 ($Q = 810$), which is dictated primarily by the coupling. Scattering-limited losses are estimated at 11% per round trip. Also displayed in the figure is the phase response obtained from a fit to the data that displays increased sensitivity near each of the two resonances.

Next, the intensity-dependent transmission of the REMZ interferometer was measured with a 10-Hz 30-ps Nd:YAG-pumped optical parametric generator (Ekspla) source at $1.545 \mu\text{m}$. The low average power of the source ensured that thermal effects could be ignored. Optical self-switching was clearly observed in some samples. Figure 6 displays transverse slices of the imaged outputs of the REMZ interferometer in Fig. 3(b). Three traces are shown, each with increasing pulse energies. Incomplete extinction resulted from higher losses in the arm containing the ring. The actual pulse energies injected into the resonators were of the order of 1 nJ. The relative distribution of output power is clearly seen to shift from one output guide to the other as the pulse energy is increased, implying a phase-shift advance of approximately π rad.

In conclusion, we have demonstrated the potential of ring resonators as nonlinear phase-shifting elements for photon energies below the half-gap. At these energies optical nonlinearities are essentially instan-

taneous, and one- and two-photon absorption and carrier generation are negligible. Our experiments show that previous demonstrations of large nonlinear phase shifts in 5-mm or longer waveguide lengths^{13,14} can be compressed into devices 100 or more times shorter. Ultracompact devices constructed from these building blocks have the potential to be engineered into ultrafast nonlinear photonic devices that generate negligible heat. For example, a device similar to the one presented in this Letter with a finesse of 100 could support 12.5-ps pulses and switch with energies as low as 4 pJ. Further optimization of the guiding confinement area and nonlinear response can produce devices with a 1-THz bandwidth and a 1-pJ energy threshold.

This work was sponsored by the Defense Advanced Research Projects Agency under grant MDA972-00-1-0021 and the New York State Office of Science, Technology and Academic Research as part of the Alliance for Nanomedical Technologies. The work was performed in part at the Cornell NanoScale Science and Technology Facility. We thank Mike Koch, Alan Bleier, John Treichler, and Rob Ilic for assistance with the fabrication. J. Heebner's e-mail address is heebner1@llnl.gov.

*Present address, Lawrence Livermore National Laboratory, L-464, 7000 East Avenue, Livermore, California 94550.

†Present address, Intel Corporation, 2501 NW 229th Avenue, M/S RA3-353, Hillsboro, Oregon 97124.

References

1. B. E. Little and S. T. Chun, *Opt. Photon. News* **11**(11), 24 (2000).
2. R. Grover, V. Van, T. A. Ibrahim, P. P. Absil, L. C. Calhoun, F. G. Johnson, J. V. Hryniewicz, and P.-T. Ho, *J. Lightwave Technol.* **20**, 900 (2002).
3. C. K. Madsen and J. H. Zhao, *Optical Fiber Design and Analysis: a Signal Processing Approach* (Wiley, New York, 1999).
4. G. Lenz, B. J. Eggleton, C. K. Madsen, and R. E. Slusher, *IEEE J. Quantum Electron.* **37**, 525 (2001).
5. S. Blair and Y. Chen, *Appl. Opt.* **40**, 570 (2001).
6. R. W. Boyd and J. E. Heebner, *Appl. Opt.* **40**, 5742 (2001).
7. J. E. Heebner, R. W. Boyd, and Q. Park, *J. Opt. Soc. Am. B* **19**, 722 (2002).
8. J. E. Heebner and R. W. Boyd, *SPIE Proc.* **4969**, 185 (2003).
9. T. A. Ibrahim, V. Van, and P.-T. Ho, *Opt. Lett.* **27**, 803 (2002).
10. V. Mizrahi, K. W. DeLong, G. I. Stegeman, M. A. Saifi, and M. J. Andrejco, *Opt. Lett.* **14**, 1140 (1989).
11. J. E. Heebner and R. W. Boyd, *Opt. Lett.* **24**, 847 (1999).
12. R. Grover, T. A. Ibrahim, T. N. Ding, Y. Leng, L.-C. Kuo, S. Kanakaraju, K. Amarnath, L. C. Calhoun, and P.-T. Ho, *IEEE Photon. Technol. Lett.* **15**, 1082 (2003).
13. S. T. Ho, C. E. Socolich, M. N. Islam, W. S. Hobson, A. F. J. Levi, and R. E. Slusher, *Appl. Phys. Lett.* **59**, 2558 (1991).
14. A. Villeneuve, C. C. Yang, P. G. J. Wigley, G. I. Stegeman, J. S. Aitchison, and C. N. Ironside, *Appl. Phys. Lett.* **61**, 147 (1992).